Millisecond-Lived Circular Rydberg Atoms in a Room-Temperature Experiment

H. Wu, R. Richaud, J.-M. Raimond, M. Brune, and S. Gleyzes
Laboratoire Kastler Brossel, Collège de France, CNRS, ENS-Université PSL, Sorbonne Université, 11, place Marcelin Berthelot, 75005 Paris, France

(Received 1 June 2022; accepted 20 December 2022; published 12 January 2023)

Circular Rydberg states are excellent tools for quantum technologies, with large mutual interactions and long lifetimes in the tens of milliseconds range, 2 orders of magnitude larger than those of laser-accessible Rydberg states. However, such lifetimes are observed only at zero temperature. At room temperature, blackbody-radiation-induced transfers cancel this essential asset of circular states, which have thus been used mostly so far in specific, complex cryogenic experiments. We demonstrate here, on a laser-cooled atomic sample, a circular state lifetime of more than 1 millisecond at room temperature for a principal quantum number 60. A simple plane-parallel capacitor efficiently inhibits the blackbody-radiation-induced transfers. One of the capacitor electrodes is fully transparent and provides large optical access to the atoms. This result paves the way to a wide range of quantum metrology and quantum simulation room-temperature experiments with long-lived, trapped circular Rydberg atoms in inhibition capacitors with full optical access.

DOI: 10.1103/PhysRevLett.130.023202

Rydberg atoms [1] are remarkable tools for quantum technologies [2–4], due to their large sensitivity to external fields and large mutual dipole-dipole interactions [5,6]. They are extensively used for the development of quantum-enabled sensors [7–10]. They led to spectacular developments for the quantum simulation of spin arrays [11,12]. Most of those experiments are based on "ordinary" low-angular-momentum Rydberg states, with a principal quantum number n of a few tens. They are easily accessible from the ground state by laser excitation. Even in a zero-temperature environment, these levels decay relatively rapidly through the emission of optical photons. This is a limitation for some experiments, from metrology to quantum simulations involving large atom numbers.

The circular Rydberg states, with maximum orbital ℓ and magnetic m quantum numbers ($\ell = m = n - 1$), have a much longer lifetime [13]. The nC circular state only decays, in a zero-temperature environment, by the emission of a millimeter-wave photon on the transition toward $(n-1)C$ ($\lambda = 9.6$ mm for $n = 60$). This photon is σ^+ polarized with respect to the quantization axis perpendicular to the electron orbit plane. This single low-frequency decay channel makes the spontaneous emission lifetime 2 orders of magnitude longer than that of ordinary Rydberg levels (∼71 ms for $60C$ and ∼500 μs for $60P$ at zero temperature).

Unfortunately, at room temperature, hundreds of photons per mode in the millimeter-wave blackbody radiation (BBR) stimulate upward and downward transitions out of the circular states. They considerably reduce their lifetime, which becomes similar to that of low-angular momentum states (∼170 μs for $60C$ and ∼140 μs for $60P$ at 300 K [14]). So far, this limitation has mostly confined circular Rydberg atoms to specific, quite complex cryogenic experiments [15].

However, BBR transfers (and even spontaneous emission) can be efficiently inhibited by placing the atoms in a conducting structure below cutoff for most of the relevant frequencies and polarizations [16–18]. Spontaneous emission inhibition has been observed on a wide variety of systems since the mideighties [19–27]. In the case of circular states, since the main transitions out of nC are in the millimeter-wave domain, a simple millimeter-size plane-parallel capacitor, perpendicular to the quantization axis, with a spacing d lower than half the wavelength of all the main σ–polarized transitions departing from the circular state, is sufficient to shield the atom from the BBR. The ability to control their decay channels resulted recently in a renewed interest in circular Rydberg atoms for quantum simulation [28–30].

In this Letter, we report the observation of the efficient inhibition of BBR-induced transfers for circular Rydberg atoms with $n \simeq 60$, prepared out of a laser-cooled cloud of rubidium atoms in an inhibition capacitor made up of indium-tin-oxide (ITO)-coated glass facing a gold-plated mirror. We observe lifetimes up to 1.1 milliseconds, 1 order of magnitude larger than those in free space, and close to the values achieved in a finite-temperature cryogenic environment [31]. One of the capacitor plates being optically transparent, it provides a wide optical access to the inhibition region, an essential feature for quantum technologies.

The experimental setup is sketched in Fig. 1(a). The capacitor is made up of an ITO-coated glass plate facing a

gold-plated copper electrode, both orthogonal to the vertical axis Oz. A square with lateral size $a = 10$ mm on the gold-plated electrode defines the inhibition region. The capacitor spacing is $d = 4.1(0.2)$ mm. A static electric field along Oz defines the quantization axis for the atom. For an infinite, ideal capacitor with the same spacing, the BBR-induced transfers out of state nC are efficiently inhibited for $n \geq 58$ [32]. The setup is contained in a rectangular glass cell, evacuated to 3×10^{-9} mbar, in which a continuously operated rubidium dispenser provides a background rubidium pressure. The ^{85}Rb atoms are continuously cooled in a standard mirror-magneto-optical trap (MOT) using two counterpropagating 45° beams, sent through the transparent ITO electrode, and reflecting on the gold-plated one, and two counterpropagating horizontal beams sent through the capacitor spacing. The MOT cloud has a size of about 1 mm.

We excite atoms from the MOT into the $58C$ circular state (for details, see the Supplemental Material [32]). The scheme begins with a pulsed, stepwise laser excitation toward $58f, m = 2$ in the presence of an electric field $\mathbf{F}$ along Oz. The excitation lasers [Fig. 1(a)] define inside the MOT a $250 \times 450 \times 250$ μm^3 excitation volume.

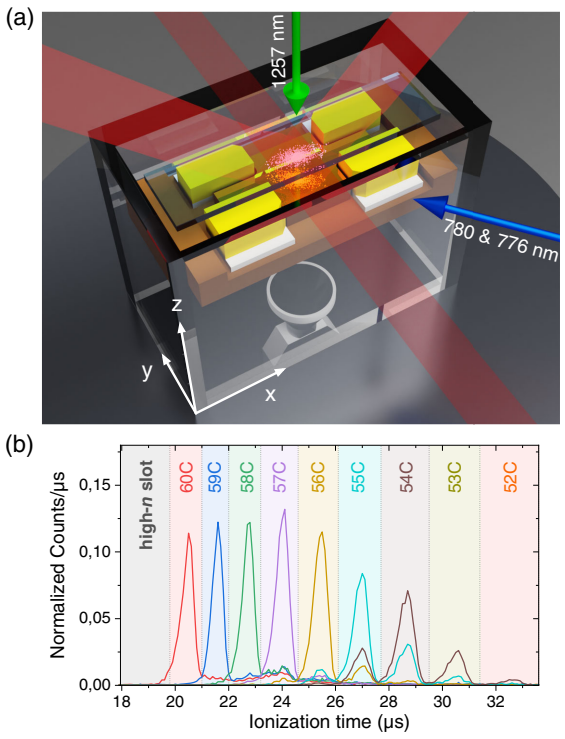

FIG. 1. (a) Scheme of the central part of the experiment. The atoms (red particles) are trapped by laser beams (dark red) in a mirror-MOT at the center of a capacitor made up of the transparent, ITO-coated glass and of a gold-plated electrode. Additional electrodes on the side (yellow) provide the rf field for circular state preparation. The Rydberg excitation lasers are shown as blue and green arrows. The axes are shown in the bottom left. (b) Ionization signals at $\tau = 0$ for all the prepared circular states.

The "circularization" procedure, thoroughly described elsewhere [35], is based on a rapid adiabatic passage between levels of the Stark manifold induced by a σ^+–polarized rf field generated by four electrodes on the sides of the inhibition capacitor [Fig. 1(a)]. It transfers the $58f, m = 2$ atoms into $58C$. Note that dc voltages also applied on the rf electrodes are set to reduce residual stray field gradients. From the $58C$ level, we transfer the atom into the circular levels from $54C$ to $60C$ using microwave (mw) π pulses. We get rid of spurious population in unwanted levels using a combination of rf pulses and partial ionization [32]. The end of the preparation process, defining the time origin $t = 0$ for the lifetime measurements, occurs at most 89 μs after the excitation laser pulse.

After a variable delay τ, the atoms are detected. An electric field ionization ramp, starting at $t = \tau$, is applied across the capacitor, reaching the ionization thresholds of different circular states at different times. The resulting ions are sent to a channeltron detector through a 0.2 mm diameter hole, drilled in the bottom plate of the capacitor. We record the number of detected ions as a function of the ionization time, defined as the time delay with respect to the trigger of the ionization ramp. All relevant levels are ionized before $t = \tau + 40$ μs. We detect at most 0.25 ion per preparation sequence. We have checked that the measured dynamics does not appreciably change when the detected atom count is reduced down to 0.05 per preparation [32]. The Rydberg density is thus low enough to preclude any influence of Rydberg-Rydberg interactions.

Figure 1(b) presents the ionization signals versus ionization time for all prepared circular states ($n = 54$ to 60) at zero delay ($\tau = 0$). The ionization peaks corresponding to different nC states are clearly separated. From the relative areas of the different peaks, we estimate the purity of the circular state preparation. It is typically between 60% and 80%, mostly limited by residual electric field gradients and by the efficiency of the mw transfer pulses. It goes down to ~50% for $n \sim 54$–55 due to the BBR field that redistributes the population into other Rydberg manifolds between the preparation and the ionization time [32].

For each initial circular state, nC, we record ionization signals for different delays τ, up to 900 μs. During this delay, BBR-induced transfers redistribute the Rydberg population among neighboring n manifolds. Simultaneously, atom cloud expansion due to its finite temperature, and possibly other loss mechanisms contribute to an overall reduction of the total number of detected ions by a factor of ~3 in 900 μs [32]. We get rid of these losses by renormalizing, for each delay, the total ion count of all detected Rydberg levels to 1. Figure 2(a) shows grayscale map plots of the normalized ion signal versus τ for the initial nC states with $n = 54$, 56, 58, and 60. For levels $54C$ and $56C$, we observe a fast redistribution among neighboring manifolds due to the strong BBR-induced transitions. For $58C$ and $60C$, this redistribution is much slower, pointing to a strong inhibition of the BBR-induced transfer rates.

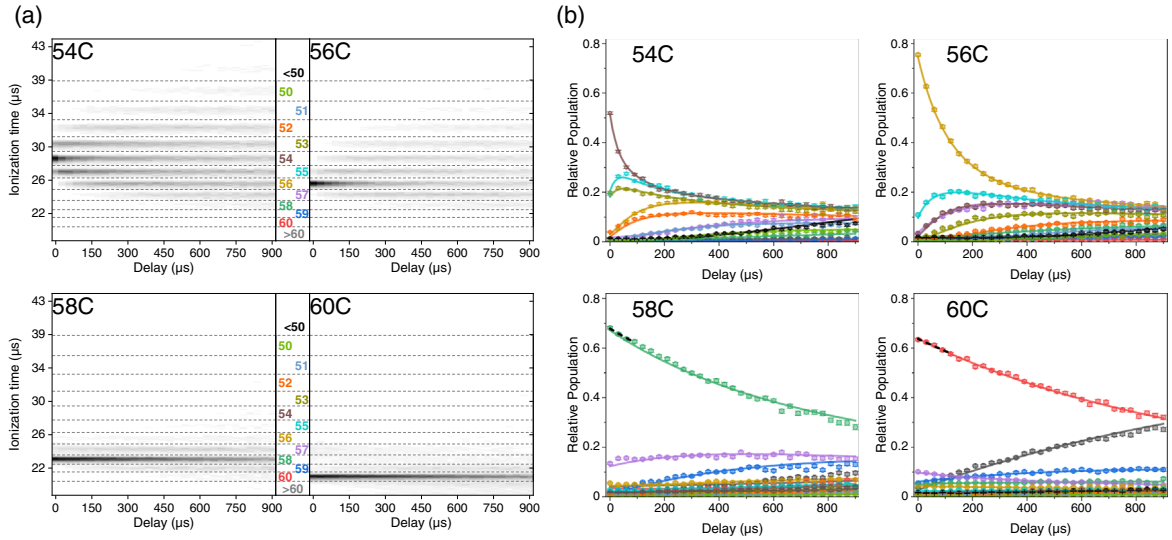

FIG. 2. (a) Grayscale plots of the ionization signal as a function of the delay τ for different initial levels ($54C$, $56C$, $58C$, and $60C$). For each panel, the grayscale is normalized to the maximum value of the signal at $\tau = 0$. Dashed lines represent the time windows used to calculate the population of each manifold. They are labeled by the corresponding value of n between 50 and 60. Levels with $n > 60$ or $n < 50$ are grouped in two broad detection windows. (b) Evolution of the populations of all levels for the same datasets. The color code is given by the color of the labels of the detection windows in (a). The points are experimental, with statistical error bars. Each point corresponds to the detection of 1800 to 9000 ions. The solid lines correspond to the results of the rate equation model fit. The thick black dashed lines show an exponential fit at short times of the prepared state population decay for $n = 58$ and $n = 60$.

From these data, we get the population of a given manifold by summing the ionization signal over the detection window defined in Fig. 2(a). Figure 2(b) shows the evolution of the populations of all manifolds for n varying from 50 to 60 as a function of time. For n's which are > 60 or < 50, we use two broad detection windows. The slow evolution of the inhibited levels, $58C$ and $60C$, is conspicuous. From a simple exponential fit to the $60C$ decay at short delays (so that only 10% of the initial population is lost, making transfers back from neighboring states negligible), we estimate the lifetime of $60C$ to be 1.3 ms, about 7.6 times that in free space at room temperature.

In order to get a more quantitative estimate of the inhibition efficiency, we record similar data as a function of τ for all initial states between $54C$ and $60C$ and fit them on a simple rate equation model for the BBR-induced transfers between adjacent manifolds. An atom in the nC state can only decay into the circular state $(n-1)C$. In contrast, absorption of a thermal photon can bring the atom in $(n+1)C$, but can also transfer the atom in a noncircular ("elliptical") state which ionizes in similar fields as the circular state of the same manifold. Because of the ratio of the matrix elements, these transfers to noncircular states are negligible in the absence of inhibition. As a result, for the initial levels with $n \leq 56$, the population dynamics is dominated by the $nC \leftrightarrow (n \pm 1)C$ transfers. Besides, since the number of thermal photons per mode, n_{th}, is high at room temperature, the upward and downward transition rates on the $nC \leftrightarrow (n+1)C$ transition are nearly equal. We thus use their common value as a single fit parameter. For higher quantum numbers, the circular to circular transitions are strongly inhibited. Transitions toward elliptical levels are no longer negligible, and upward transfer rates become larger than downward rates. We model this asymmetry by using different fit parameters for upward and downward transition rates between manifolds n and $(n+1)$ for $n \geq 57$.

We also use different upward and downward rates for the transfers into the slots gathering all levels above $60C$ and below $50C$ (these slots include many levels, and the return rate from them is clearly different from the departure rate into them). We fit as free parameters the initial population of each circular state for each dataset (for details on the fitting procedure, see the Supplemental Material [32]). The solid lines in Fig. 2(b) present the population evolution resulting from this fit. They are in excellent agreement with the experimental values.

Figure 3 presents the corresponding transfer rates and compares them to the values calculated from a numerical simulation performed with CST Studio [32,36] taking into account the actual electrode structure and assuming a BBR temperature of 300 K. The simulated rates are in fair agreement with the fitted ones. Around $\lambda = 7.4$ mm, we observe that the capacitor structure enhances the transition rates as compared with those in free space (black line). In this region, the simulation correctly predicts an enhancement, although it underestimates its effect. This can be explained by an imperfect modeling of the exact resonance of the electrode structure or by a larger microwave field

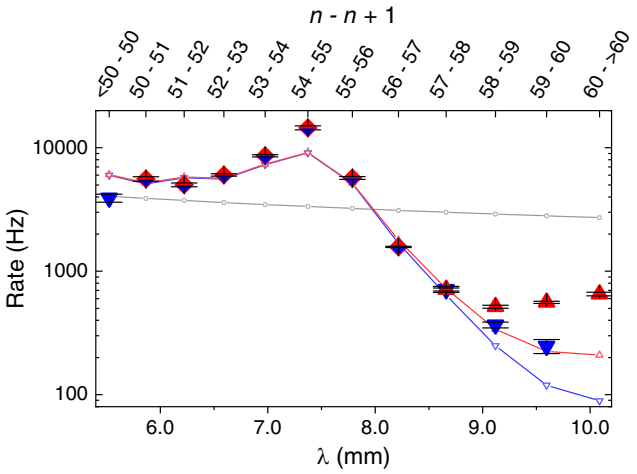

FIG. 3. Transfer rates between manifolds (labeled on the upper scale). The lower scale shows the $nC \leftrightarrow (n+1)C$ transition wavelength λ. The solid symbols show the rates obtained from the fit, with statistical error bars deduced from fits to subensembles of the data (see the Supplemental Material [32]). Blue downward triangles and red upward triangles show the $(n+1) \rightarrow n$ and $n \rightarrow (n+1)$ rates respectively. Two-color diamonds show the $n \leftrightarrow (n+1)$ rates when upward and downward rates are assumed to be equal in the model. The transfer rates back from the collective detection window for high n ("> 60") or for low n ("< 50") are not plotted. The open symbols result from numerical simulations. The blue open triangles give the $nC \leftrightarrow (n+1)C$ rates. The red open triangles give the $n \rightarrow (n+1)$ rates when taking into account transfers to the elliptical states. The gray circles present the calculated free-space rates. The blue, red, and gray lines are guides to the eye.

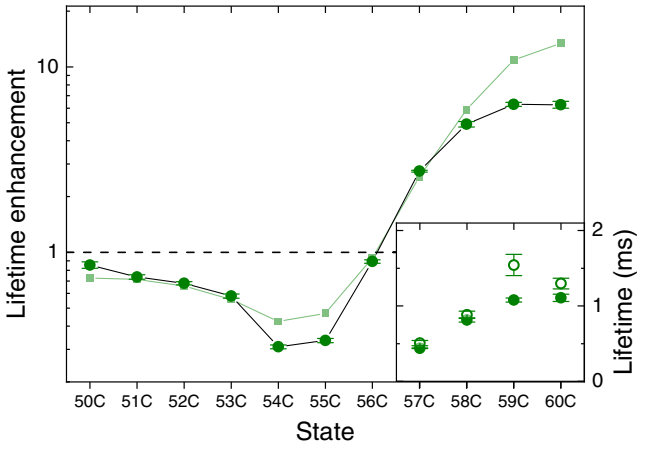

FIG. 4. Lifetime enhancement of the circular states. Full green circles show the measured lifetimes in capacitor normalized to the calculated free-space lifetimes at 300 K. The square points show the same ratio predicted by the numerical simulation. Inset: lifetime of the circular states, deduced from the rate equation fit (solid points) or from the exponential fit of the circular state population decay at short delays (open points). All error bars are deduced from the fit uncertainties.

temperature due to the presence of the hot rubidium dispenser inside the UHV chamber [32].

For $n \geq 56$, the rates are well below the free-space ones, although they are slightly higher than the simulated values. This discrepancy can be explained by a combination of experimental imperfections, including in particular a thermal BBR temperature higher than 300 K [32], by spurious mw resonances of the structure, by an imperfect ITO coating, or simply by the cloud thermal expansion, which limits the measurement precision for the lowest rates. In spite of these imperfections, the experiment clearly demonstrates thermal transfer inhibition. For strongly inhibited transitions, the upward rates are higher than the downward rates. This is consistent with the fact that upward transitions toward elliptical levels significantly come into play. For the $59 \leftrightarrow 60$ transition, the difference between the upward and downward rates is 0.31(3) kHz. It is close to the rate of thermal transfer from $59c$ toward the noncircular state predicted by the simulation (≈0.17 kHz). Our simplified model is thus sufficient to capture the dynamics in the inhibition region.

Finally, we sum the fitted rates $n \rightarrow (n \pm 1)$ to get the total lifetimes of the nC states normalized to the calculated free-space lifetimes at 300 K (green dots in Fig. 4). All the measured lifetime enhancements agree quite well with the simulation results (green line). They are, for the inhibited states, in very good agreement with the estimated lifetime directly based on the exponential fit at short delays (open green dots in the inset). We observe lifetimes (inset in Fig. 4) up to 1.1 ± 0.1 ms for $n = 60$.

We have observed, at room temperature, circular states' lifetimes in the millisecond range. They are nearly 1 order of magnitude larger than in free space and comparable to those observed in a cryogenic environment [31]. This proof-of-principle experiment shows that transparent, conductive electrodes provide a large inhibition while offering a wide optical access to the atoms.

The preparation fidelity could be improved by a better control of stray fields and the use of advanced quantum control techniques for the circularization process [37]. Field-ionization detection could be replaced by a direct optical detection of the circular atoms through a transfer back to the ground state or through the use of the optically active electron of an alkaline earth circular state [38,39].

One can thus envision circular atoms laser trapped [40] in complex arrangements of optical tweezers [29,30] inside an inhibition capacitor made up of two transparent electrodes. Ideally, with a larger capacitor made up of two ITO plates (40 mm transverse dimension), lifetimes up to 6 ms could be obtained, limited by residual upward uninhibited transitions. Geometrically more complex transparent 3D structures also inhibiting these transitions could lead to even longer lifetimes. These results thus open the way for a widespread use of circular atoms in existing and future Rydberg experiments.

We thank Rodrigo Cortiñas, Brice Ravon, and Igor Dotsenko for experimental support, and Fernando Gago

for fruitful discussions. We acknowledge support from the European Union's Horizon 2020 under Grant Agreement No. 786919 (TRENSCRYBE) and from the Agence Nationale de la Recherche under Project No. 167754 (SNOCAR). H. W. acknowledges support of a China Scholarship Council No. 201806190206.

[1] T. F. Gallagher, *Rydberg Atoms* (Cambridge University Press, Cambridge, 1994).
[2] M. Saffman, T. G. Walker, and K. Mølmer, Rev. Mod. Phys. **82**, 2313 (2010).
[3] M. Saffman, J. Phys. B **49**, 202001 (2016).
[4] C. S. Adams, J. D. Pritchard, and J. P. Shaffer, J. Phys. B **53**, 012002 (2020).
[5] M. D. Lukin, M. Fleischhauer, R. Côté, L. M. Duan, D. Jaksch, J. I. Cirac, and P. Zoller, Phys. Rev. Lett. **87**, 037901 (2001).
[6] A. Browaeys and T. Lahaye, Nat. Phys. **16**, 132 (2020).
[7] J. A. Sedlacek, A. Schwettmann, H. Kübler, R. Löw, T. Pfau, and J. P. Shaffer, Nat. Phys. **8**, 819 (2012).
[8] H. Fan, S. Kumar, J. Sedlacek, H. Kübler, S. Karimkashi, and J. P. Shaffer, J. Phys. B **48**, 202001 (2015).
[9] A. Facon, E.-K. Dietsche, D. Grosso, S. Haroche, J.-M. Raimond, M. Brune, and S. Gleyzes, Nature (London) **535**, 262 (2016).
[10] L. A. Downes, A. R. MacKellar, D. J. Whiting, C. Bourgenot, C. S. Adams, and K. J. Weatherill, Phys. Rev. X **10**, 011027 (2020).
[11] P. Scholl, M. Schuler, H. J. Williams, A. A. Eberharter, D. Barredo, K.-N. Schymik, V. Lienhard, L.-P. Henry, T. C. Lang, T. Lahaye, A. M. Läuchli, and A. Browaeys, Nature (London) **595**, 233 (2021).
[12] S. Ebadi, T. T. Wang, H. Levine, A. Keesling, G. Semeghini, A. Omran, D. Bluvstein, R. Samajdar, H. Pichler, W. W. Ho, S. Choi, S. Sachdev, M. Greiner, V. Vuletić, and M. D. Lukin, Nature (London) **595**, 227 (2021).
[13] J.-M. Raimond, M. Brune, and S. Haroche, Rev. Mod. Phys. **73**, 565 (2001).
[14] M. Archimi, M. Ceccanti, M. Distefano, L. Di Virgilio, R. Franco, A. Greco, C. Simonelli, E. Arimondo, D. Ciampini, and O. Morsch, Phys. Rev. A **105**, 063104 (2022).
[15] S. Haroche and J.-M. Raimond, *Exploring the Quantum: Atoms, Cavities and Photons* (Oxford University Press, New York, 2006).
[16] D. Kleppner, Phys. Rev. Lett. **47**, 233 (1981).
[17] A. G. Vaidyanathan, W. P. Spencer, and D. Kleppner, Phys. Rev. Lett. **47**, 1592 (1981).
[18] R. G. Hulet, E. S. Hilfer, and D. Kleppner, Phys. Rev. Lett. **55**, 2137 (1985).
[19] G. Gabrielse and H. Dehmelt, Phys. Rev. Lett. **55**, 67 (1985).
[20] D. J. Heinzen, J. J. Childs, J. E. Thomas, and M. S. Feld, Phys. Rev. Lett. **58**, 1320 (1987).
[21] W. Jhe, A. Anderson, E. A. Hinds, D. Meschede, L. Moi, and S. Haroche, Phys. Rev. Lett. **58**, 666 (1987).
[22] G. Björk, S. Machida, Y. Yamamoto, and K. Igeta, Phys. Rev. A **44**, 669 (1991).
[23] S. Haroche, in *Fundamental Systems in Quantum Optics, Les Houches Summer School, Session LIII*, edited by J. Dalibard, J.-M. Raimond, and J. Zinn-Justin (North Holland, Amsterdam, 1992), p. 767.
[24] K. Tanaka, T. Nakamura, W. Takamatsu, M. Yamanishi, Y. Lee, and T. Ishihara, Phys. Rev. Lett. **74**, 3380 (1995).
[25] M. Bayer, T. L. Reinecke, F. Weidner, A. Larionov, A. McDonald, and A. Forchel, Phys. Rev. Lett. **86**, 3168 (2001).
[26] P. Lodahl, A. F. van Driel, I. S. Nikolaev, A. Irman, K. Overgaag, D. Vanmaekelbergh, and W. L. Vos, Nature (London) **430**, 654 (2004).
[27] A. Bienfait, J. J. Pla, Y. Kubo, X. Zhou, M. Stern, C. C. Lo, C. D. Weis, T. Schenkel, D. Vion, D. Esteve, J. J. L. Morton, and P. Bertet, Nature (London) **531**, 74 (2016).
[28] T. L. Nguyen, J. M. Raimond, C. Sayrin, R. Cortiñas, T. Cantat-Moltrecht, F. Assemat, I. Dotsenko, S. Gleyzes, S. Haroche, G. Roux, T. Jolicoeur, and M. Brune, Phys. Rev. X **8**, 011032 (2018).
[29] F. Meinert, C. Hölzl, M. A. Nebioglu, A. D'Arnese, P. Karl, M. Dressel, and M. Scheffler, Phys. Rev. Res. **2**, 023192 (2020).
[30] S. R. Cohen and J. D. Thompson, PRX Quantum **2**, 030322 (2021).
[31] T. Cantat-Moltrecht, R. Cortiñas, B. Ravon, P. Méhaignerie, S. Haroche, J. M. Raimond, M. Favier, M. Brune, and C. Sayrin, Phys. Rev. Res. **2**, 022032(R) (2020).
[32] See Supplemental Material at http://link.aps.org/supplemental/10.1103/PhysRevLett.130.023202, which includes Refs. [33,34], for additional information on the preparation of the initial states, the experimental details, the model and CST calculations and the fitting procedures.
[33] C. Hermann-Avigliano, R. C. Teixeira, T. L. Nguyen, T. Cantat-Moltrecht, G. Nogues, I. Dotsenko, S. Gleyzes, J. M. Raimond, S. Haroche, and M. Brune, Phys. Rev. A **90**, 040502(R) (2014).
[34] E. A. Hinds, in *Advances in Atomic and Molecular Physics*, edited by D. Bates and B. Bederson (Academic Press, San Diego, 1990), Vol. 28, p. 237.
[35] A. Signoles, E. K. Dietsche, A. Facon, D. Grosso, S. Haroche, J. M. Raimond, M. Brune, and S. Gleyzes, Phys. Rev. Lett. **118**, 253603 (2017).
[36] https://www.3ds.com/products-services/simulia/products/cst-studio-suite/.
[37] A. Larrouy, S. Patsch, R. Richaud, J.-M. Raimond, M. Brune, C. P. Koch, and S. Gleyzes, Phys. Rev. X **10**, 021058 (2020).
[38] A. Muni, L. Lachaud, A. Couto, M. Poirier, R. C. Teixeira, J.-M. Raimond, M. Brune, and S. Gleyzes, Nat. Phys. **18**, 502 (2022).
[39] J. T. Wilson, S. Saskin, Y. Meng, S. Ma, R. Dilip, A. P. Burgers, and J. D. Thompson, Phys. Rev. Lett. **128**, 033201 (2022).
[40] R. G. Cortiñas, M. Favier, B. Ravon, P. Méhaignerie, Y. Machu, J. M. Raimond, C. Sayrin, and M. Brune, Phys. Rev. Lett. **124**, 123201 (2020).